Materials & Design 230 (2023) 111975

Contents lists available at ScienceDirect

Materials & Design

journal homepage: www.elsevier.com/locate/matdes

# Efficient optimization framework for L-PBF fatigue enhanced Ti6Al4V lattice component

Raffaele De Biasi [a,*], Simone Murchio [a,b], Elia Sbettega [c], Simone Carmignato [c], Valerio Luchin [d], Matteo Benedetti [a]

[a] Department of Industrial Engineering, University of Trento, Trento, Italy
[b] BIOtech Research Center, University of Trento, Trento, Italy
[c] Department of Management and Engineering, University of Padua, Vicenza, Italy
[d] Lincotek Additive, Pergine Valsugana, Italy

## HIGHLIGHTS

- A novel cost-effective optimization framework for fatigue life improvement is proposed for metallic lattice structure components.
- Lattice component fatigue life is improved acting on specimen printing orientation.
- An improvement of +24 % in the fatigue life is experimentally achieved.
- Fatigue life of lattice components is estimated from experimentally measured miniaturized specimens' data.

## GRAPHICAL ABSTRACT

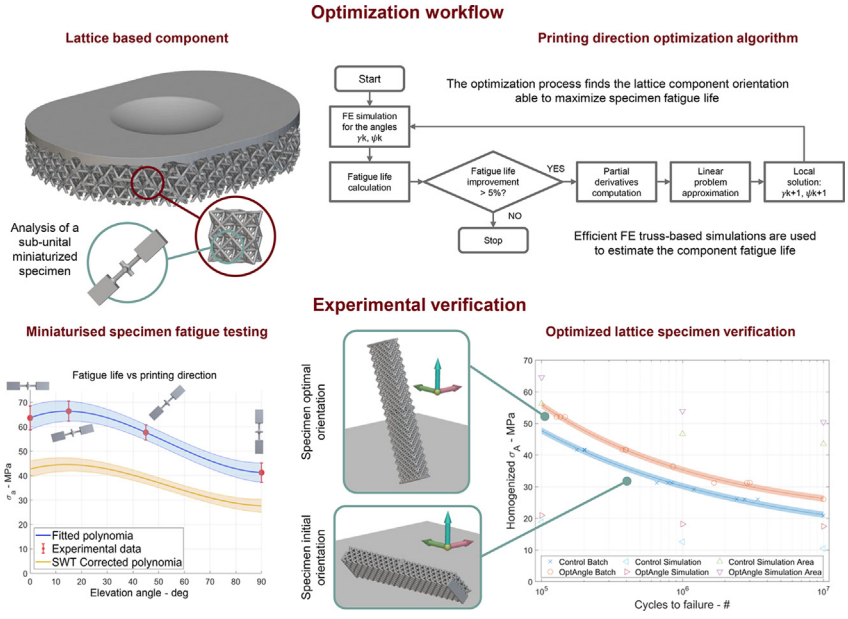


## ARTICLE INFO

*Article history:*
Received 7 February 2023
Revised 11 April 2023
Accepted 26 April 2023
Available online 2 May 2023

*Keywords:*
Lattice structure
Fatigue life optimisation
Laser powder bed fusion

## ABSTRACT

Industries today face challenges in incorporating metallic additively manufactured lattice structures in critical components subjected to fatigue loading. This work explores the relationship between fatigue properties and the printing orientation of Laser-Powered Bed Fusion (LPBF) lattice structures. This relation is at the base of a cost-effective and time-efficient optimization workflow able to determine the optimal lattice printing orientation for improved fatigue life. Fatigue resistance is tested under uniaxial conditions on miniaturized specimens that mimic the lattice sub-unit elements: struts and nodes. The collected data is used as input for the optimization algorithm to determine the specimen orientation that maximizes fatigue life. The optimized specimens are manufactured, tested under three-point-bending conditions, and analysed using metrological x-ray computed tomography to verify the improvement.

* Corresponding author.
*E-mail address:* raffaele.debiasi@unitn.it (R. De Biasi).

https://doi.org/10.1016/j.matdes.2023.111975
0264-1275/© 2023 The Author(s). Published by Elsevier Ltd.
This is an open access article under the CC BY-NC-ND license (http://creativecommons.org/licenses/by-nc-nd/4.0/).

Printing orientation
Fatigue testing and verification
Miniaturised specimens

The proposed workflow is able to produce a 24 % increase in specimen fatigue life by simply adjusting the orientation on the printing plane.

© 2023 The Author(s). Published by Elsevier Ltd. This is an open access article under the CC BY-NC-ND license (http://creativecommons.org/licenses/by-nc-nd/4.0/).

## 1. Introduction

Cellular lattice materials display a large range of tuneable multifunctional properties conferred by their peculiar topology [1]. This consists in filling a 3D space with a regular and periodic pattern of undistorted unit cells, which are composed of slender straight members usually termed "struts", joined together in specific locations termed "nodes". Multifunctional properties like stiffness [2], strength [3], thermal conductivity [4], and permeability [5], turn out to be controlled by the unit cell properties (like relative porosity, strut thickness to unit cell size ratio or the strut connectivity dictated by the Maxwell stability criterion [6]) rather than by the characteristics of the base material composing the lattice. This offers the designer a broad design space, paving the way for optimised cellular lattice materials [7] that potentially can find application in a wide range of industrial fields, such as the aerospace and the biomedical industries [8,9]. Unfortunately, the poor fatigue properties of cellular lattice materials are a well-known Achilles' heel [10], fuelling widespread concern about the structural integrity of this class of materials under time-varying loads. As a consequence, industry is still distrusting their extensive use in critically loaded mechanical components and it is waiting for solid answers and guidance in this regard. The cause of the lower fatigue properties is twofold. First, the architecture of cellular materials itself is an intrinsic factor of structural weakening, since a full geometry is replaced by a porous arrangement of struts. This can lead to a reduced load bearing area and to increased stress concentrations at the nodes [11]. Second, additive manufacturing (AM) techniques - such as L-PBF - employed in the cellular lattice fabrication, inevitably introduce manufacturing imperfections, detrimentally impacting on the fatigue strength of the entire component [12,13]. The most significant fatigue-related manufacturing defects found in metallic lattices are internal pores and surface irregularities, often referred to as notches [14,15]. These imperfections are not evenly distributed throughout the lattice and are strongly influenced by the orientation of the strut relative to the building plane. [16]. It is widely known that inclined struts are supported by loose powder with lower thermal conductivity compared to the bulk material. As a result, inclined struts have a higher fraction of partially or completely melted powder than vertical struts. This leads to different thermal conditions depending on the printing orientation, causing the formation of varying internal defects and diverse irregular surface morphologies [17,18]. In this scenario, the direct design of a fatigue-improved lattice structure before the manufacturing stage could be of enormous advantage for a more robust and faster scale-up of metal AM to the industrial field.

Structural optimization and topology optimization techniques are indeed gaining increasing interest in recent years due to the design freedom given by the AM process. The usage of an optimization process in a lattice structure is extensively covered in the literature [19] and it generally aims to improve the mechanical properties of the lattice. Authors like Cheng et al. [20], Khanoki and Pasini [21], Fernandez and Tamijani [22] and Gorguluarslan et al. [23] focused on a homogenization-based topology optimization to achieve lightweight design and synthesize graded lattice structures. A common feature in their work is the crucial role that lattice modelling plays in the optimization process. Computational efficiency is a core requirement in their framework, and it is achieved through the use of homogenized models that reduce the geometric complexity inherent in porous materials.

The importance of the lattice orientation in the design of a component is well-known and taken into consideration in several structural optimization problems [23]. However, the dependence of the fatigue material properties with respect to the printing direction is far from being integrated into an optimization algorithm.

In this work, a systematic structural optimization framework is proposed to design a fatigue-resistant lattice component. The optimization algorithm is driven by experiments, as it is based on the results of fatigue tests conducted on miniaturized specimens composed of lattice sub-unit elements. The validity of the algorithm is demonstrated through the design of a three-point bending lattice specimen that is enhanced for improved fatigue resistance. The proposed approach is also general enough to meet the needs of industrial applications, as it reduces fatigue verification costs and accommodates the design phase where time to market is a crucial requirement. To improve computational efficiency, the static analysis is performed using one-dimensional Finite Element (FE) elements instead of more demanding solid elements and topological optimization processes.

The paper is organized as follows. Section 2 provides a general description of the methodology used in the research and its constitutive steps. The first part describes the experimental fatigue campaign on miniaturized specimens and the subsequent discussion of a mathematical model that correlates the fatigue life with the printing direction. The second part explains the optimization process and the algorithm used. Section 3 focuses on specimen design and manufacturing, while Section 4 provides an interpretation of the results, including the results of X-ray computed tomography (CT) measurements and the statistical nature of the fatigue phenomenon. The paper concludes in Section 4 with the main results and limitations, as well as potential future research directions.

## 2. Materials and methods

### 2.1. Optimization framework

A structural optimization framework designed to enhance the fatigue strength of AM components by determining the best printing orientation is proposed. The optimization approach is comprehensive in scope and can be applied to a wide range of lattice components of varying shapes, geometries, and cell unit types. The main stages of this method are illustrated in Fig. 1, showcasing a potential application: a portion of a spinal prosthetic implant for disc replacement featuring an Octet Truss (OT) lattice structure on one side for better osteointegration and a solid surface on the other side for accommodating the artificial disc.

#### 2.1.1. Fatigue behaviour of miniaturised sub-unital lattice specimens

In AM components, the printing orientation is a critical factor that affects the quality of the entire lattice structure and its mechanical and fatigue properties. The surface defect distribution and the geometrical integrity of the lattice can be significantly influenced by the specimen printing direction. This work studies the impact of building orientation on the mechanical and fatigue integrity of the lattice, starting from its basic elements, struts, and nodes. Furthermore, the ability to extensively test miniatur-

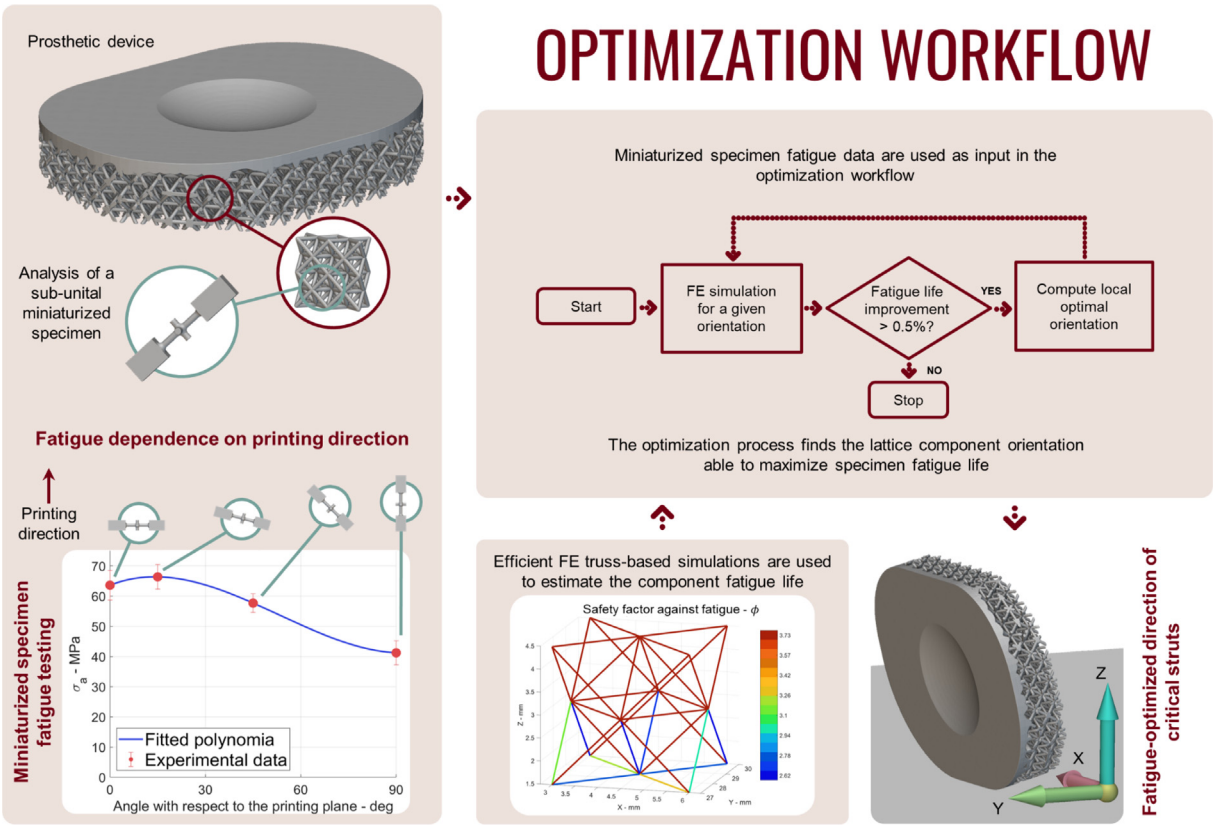


**Fig. 1.** Optimization workflow for lattice components fatigue life improvement. Fatigue properties of the lattice sub-unital elements are measured from uniaxial fatigue tests. The effect of the printing angle on the fatigue life is accessed. Based on these results, an optimization algorithm improves the fatigue resistance of the lattice component finding its optimal printing orientation in the printing chamber.

ized specimens can significantly reduce the cost and improve the efficiency of the component design and verification processes.

In the first stage of this work, an experimental fatigue campaign is conducted on miniaturized sub-unit specimens to determine the correlation between specimen fatigue resistance and their elevation angle with respect to the printing plane.

Four different micro-specimen inclinations are evaluated, and uniaxial fatigue data is analysed to establish a relationship between the inclination angle and the fatigue resistance of the specimens [24,25]. It should be noted that, to simplify the analysis, the authors will only focus on the stretched dominated cell topology, with the stresses inside the struts fully described by their axial stresses [26].

### 2.1.2. Formulation of the optimization problem

The goal of this work is to optimize the orientation of a metallic additively manufactured lattice component to improve its fatigue life. To achieve this, the authors first conduct an experimental fatigue campaign on miniaturised specimens to correlate the specimen fatigue resistance to their elevation angle with respect to the printing plane. Then, a metric to describe the fatigue life of the entire lattice component is defined based on the fatigue life of its most critical strut, since its failure can weaken the structure and lead to eventual failure of the entire lattice. The optimization process involves orienting the entire lattice component in the printing chamber to print the most critically loaded struts in the optimal orientation that maximizes their fatigue resistance. This solution does not involve any modification to the lattice design, just relying on the rotation of the overall component in the printing chamber.

To determine the probability of failure within a strut, a safety factor $\phi_i$ against fatigue is established by considering both the axial stress within the lattice struts and the fatigue resistance derived from miniaturized specimen fatigue tests. In lattice structures, buckling can also be a critical failure mechanism, so the axial stress is also compared to the Euler buckling resistance. A Finite Element (FE) linear static analysis is performed to estimate the axial stress within the lattice. The Octet truss cells can be modelled using 1D truss elements, where each strut is represented by a truss element and each node is considered as an ideal hinge [26].

The authors developed a custom FE truss solver in MATLAB R2020b (MathWorks, USA), able to analyse 2D and 3D structure modelling the structures as truss elements. An in-depth description of the Finite Element model described above is available in Appendix A, section A3.

To find the optimal spatial orientation of the entire component with respect to the printing plane, two coordinates, $\gamma$ and $\psi$ describing respectively the rotations around the X and Y axes, are defined (see Fig. 4B and C) and adopted as algorithm optimization variables. The optimization problem can therefore be formulated as follow:

$$\begin{cases} \max\limits_{\gamma,\psi} g_0(\gamma,\psi) = \max\limits_{\gamma,\psi} \min\limits_{i} \phi_i(\gamma,\psi) \\ s.t. \begin{cases} g_1(\gamma,\psi) = \phi_i \geq \phi* \\ \gamma \in S \\ \psi \in S' \end{cases} \end{cases} \quad (2)$$

where the cost function $g_0$ represents the minimum of the safety factor against fatigue among the specimen struts. This quantity needs to be maximised acting on the optimization angles. At the same time some constraints need to be satisfied: the safety factor

of each strut $\phi_i$ must be greater than a desired value $\phi^*$, and the optimization variables must assume values inside a defined set: $S$ and $S'$ respectively. The two sets can be different and can accommodate manufacturability needs such as support placement or specimen orientation to achieve the maximum usage of printing batch.

#### 2.1.3. Optimization algorithm

The solution strategy of the optimization problem relies on a gradient-based approach and on the formulation of approximated linear subproblems.

The sensitivity analysis is conducted numerically: starting from a design variable configuration, a variation $h$ is applied to each optimization angle and the partial derivative is approximated as a finite difference. Formally:

$$\frac{\partial g_n(\alpha)}{\partial \alpha_i} = \frac{g_n(\alpha + he_i) - g_n(\alpha)}{h} \tag{3}$$

where $\alpha_i$ is the *i-th* optimization variable, $g_n$ is the cost function or the constraint function and $e_i$ is a vector applying the variation $h$.

Once the sensitivity analysis is performed and all the mentioned data are retrieved, the optimization step can be rewritten as a Sequential Linear Programming (SLP) problem. As reported in Eq. (4):

$$\begin{cases} \min\limits_{\alpha} \; g_0(\alpha^k) + \nabla g_0(\alpha^k)^T(\alpha - \alpha^k) \\ s.t. \begin{cases} g_1(\alpha^k) + \nabla g_1(\alpha^k)^T(\alpha - \alpha^k) \\ \alpha \in S \\ -l_i^k \le \alpha_i - \alpha_i^k \le h_i^k \end{cases} \end{cases} \tag{4}$$

Where $\alpha^k$ is the set of the optimization variable at the step $k$ while $\nabla g_0$ and $\nabla g_1$ are the gradient of the cost function and the constraint equation. The quantities $l_i^k$ and $h_i^k$ are the lower and upper limits for the optimization variables at the step $k$.

The optimization problem in Eq. (4) can be solved using the Simplex method. This method iteratively computes the optimal configuration of variables to improve the fatigue performance of the structure locally. The process is outlined in a step-by-step algorithm, as shown in Fig. 2.

An algorithm stopping criterion has been defined as follows: the cost function value at step $k + 1$ is compared with the one at step $k$. If the improvement is below a given threshold, set in this case to 0.5 %, the algorithm stops and the optimization variables at step $k + 1$ are selected as optimal configuration.

### 2.2. Miniaturised strut-junction specimens

#### 2.2.1. Design and manufacturing

Miniaturised strut-junction specimens mimicking the lattice sub-unit nodes were designed as shown in Fig. 3. In brief, a cylindrical dog-bone thin-strut specimen with a node placed in the middle section of the gauge length was generated, considering a nominal strut diameter of 670 μm, a fillet radius at the node of 600 μm, and a total gauge length of 4000 μm.

Miniaturised specimens were manufactured by Laser-Powder Bed Fusion (L-PBF) employing a Ti6Al4V biomedical graded spherical powder ($O_2$ < 0.2 %) with a particle size in the 15–45 μm range. An EOS M290 printer equipped with a nominal laser power of 400 W was used for the fabrication of the strut-junction specimens according to four different directions, namely with an angle $\gamma$ = 90°, 45°, 15° and 0° with respect to the job plate. More details about the fabrication process and post-process treatment can be found in [27].

#### 2.2.2. Fatigue testing

The four different batches of miniaturised specimens were fatigue tested by means of a Bose Electroforce 3200, equipped with a 200 N load cell at full scale and at a 200 Hz nominal working frequency, in a sinusoidal waveform. To measure the fatigue strength of the strut-junction specimens, load-controlled fully reversed fatigue cycle tests at constant amplitude (stress ratio R = −1) were conducted till the specimen failure or upon a runout threshold set at $10^7$ cycles. At least 12 specimens per printed batch were fatigue tested in order to build the Wöhler curves of strut junction specimens according to the four building orientations. Experimental data underwent a data fitting to plot the 50 % failure probability curve, along with the 10 %–90 % failure probability scatter bands. The authors address the reader to [25], for a more in-depth discussion on the curve fitting process.

### 2.3. Three-point bending specimens

#### 2.3.1. Design and manufacturing

In this work, a three-point bending lattice specimen is designed to test the proposed method in a real-world component. The specimen is designed to have a complex combination of tensile and compressive stresses, with a compressive external load, making it easier to set up experiments. The Octet Truss (OT) cell topology is chosen, with a cell size of 3 mm and a strut diameter of 0.7 mm, resulting in a lattice porosity of 48 %. The specimen consists of a 4 × 20 × 2 array of OT cells and a bulk part that acts as reinforcement in the contact area with the testing machine. The

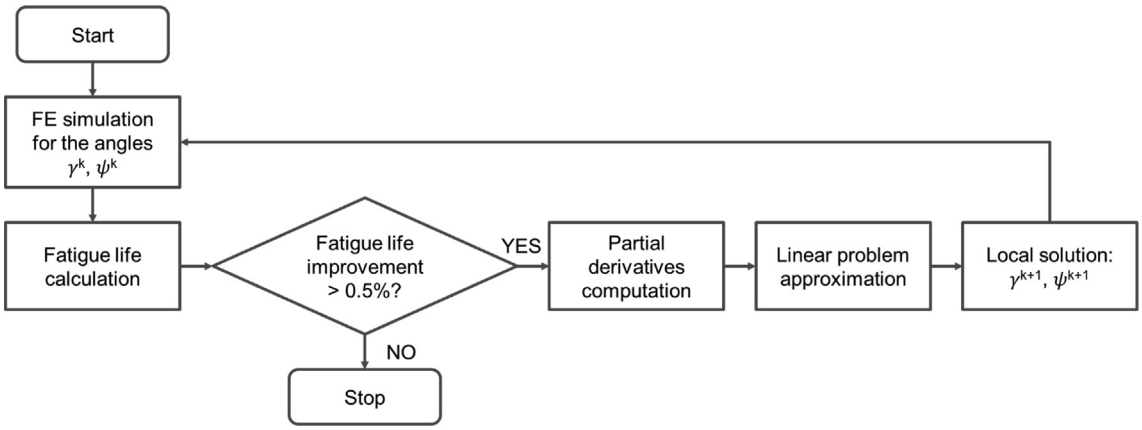


**Fig. 2.** Gradient-based optimization algorithm for lattice components fatigue life improvement. An extended version of the proposed scheme is available in Appendix C.

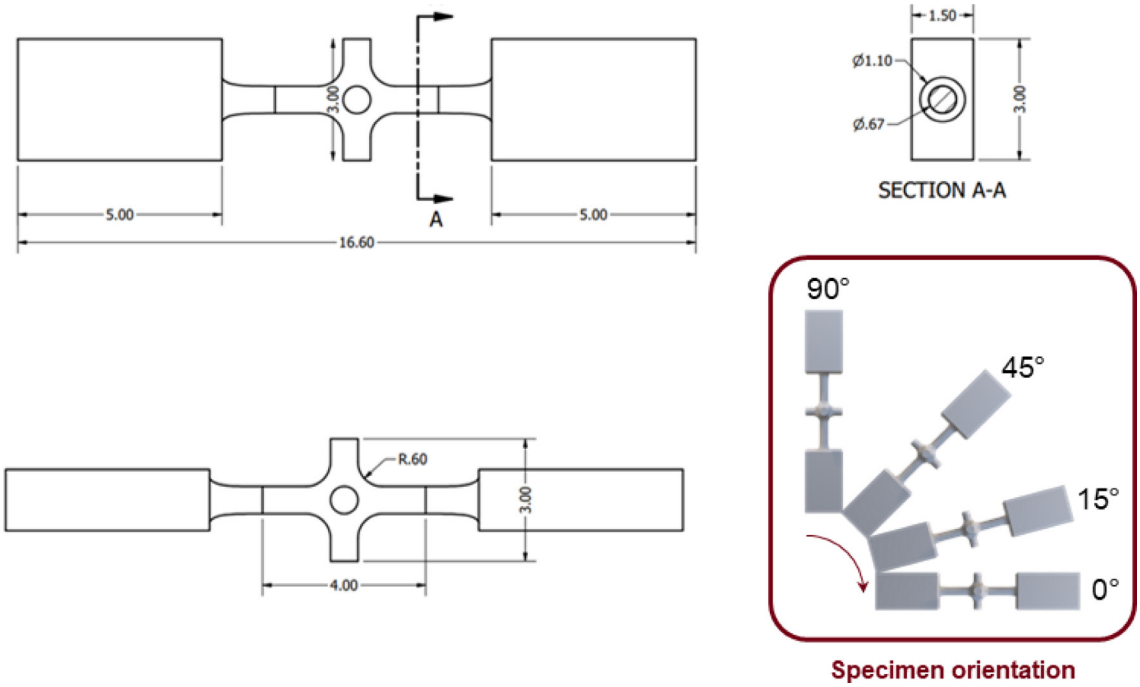


**Fig. 3.** Geometrical details of the miniaturised specimens used for the fatigue property assessments.

specimen dimensions are 12 mm × 60 mm × 6 mm. A visual representation of the specimen geometry can be seen in Fig. 4A. A more detailed description of the reinforcement design can be found in the Supplementary materials, Appendix A1 and A2.

Additionally, the orientation of a lattice structure with respect to the printing plane can be described by defining a cartesian reference frame and two angles, called γ and ψ as shown in Fig. 4B and C. The reference frame is aligned to the printing plane, reporting the vertical axis normal to the job plate.

Two different batches of specimens are manufactured by L-PBF of a Ti6Al4V biomedical graded powder. The process parameters adopted for the fabrication are the same as those used in the creation of miniaturized specimens. The "control" batch and the "optimised" batch only differ in the chosen printing spatial orientation, defined by the two angles γ and ψ. The control batch is composed of 12 OT specimens printed with a spatial orientation suggested by the company to minimise the usage of support structures. The printing orientation of these control specimens, accord-

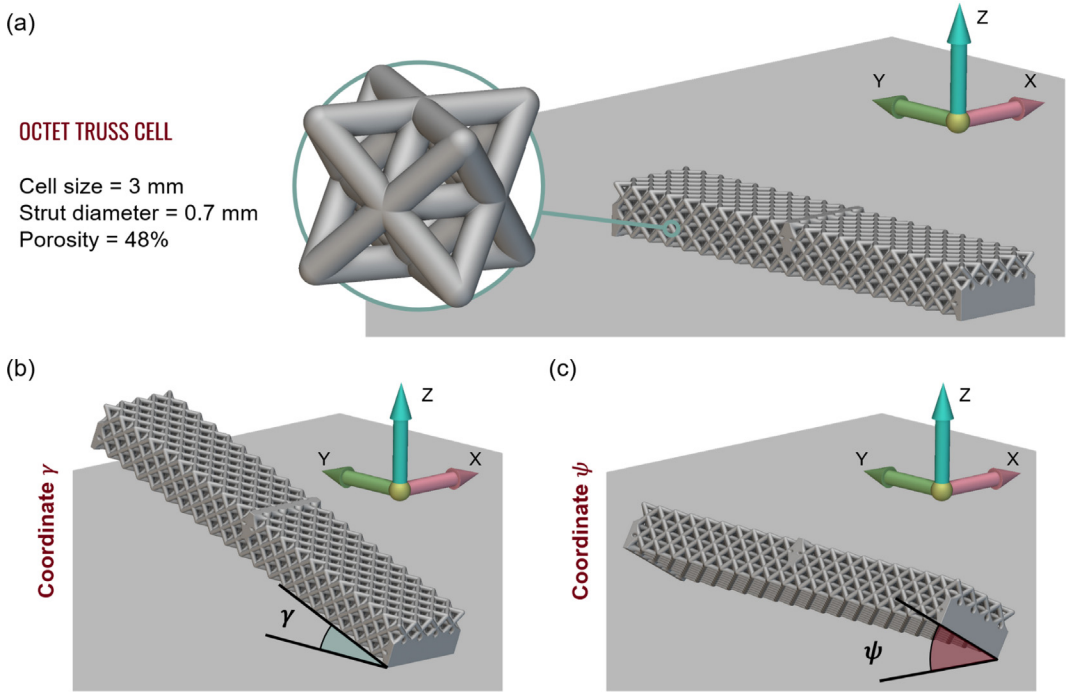


**Fig. 4.** Three-point bending specimen designed for the optimization workflow verification. A: Octet Truss (OT) cell and specimen main characteristics. The reference frame used in the analysis is depicted; B: Elevation angle γ, describes the rotation around the X axis; C: Elevation angle ψ, describes the rotation around the Y axis.

ing to the reference frame available in Fig. 6 is $\gamma = 0°$ and $\psi = 45°$. The second "optimised" batch is formed by 12 OT specimens and it is printed following the optimal printing orientation suggested by the optimization algorithm.

*2.3.2. Fatigue testing*

The fatigue resistance of the two batches of metallic lattices is evaluated through three-point-bending tests performed using a Rumul Mikroton machine equipped with a 1 kN load cell. The tests are carried out under load control, which is applied with a sinusoidal waveform at a nominal frequency of 90 Hz and a load ratio R = 0.1. The specimens are considered to have failed if the drop in testing frequency exceeds 2 Hz. The tests are terminated when the number of cycles surpasses $1 \times 10^7$. The fatigue data are fitted using the homogenized stress amplitude, $\sigma_a$, assessed in the most stressed spot of the specimen (midline outer fibre). Equation (5) computes the $\sigma_a$ stress considering the specimen as a simply beam. $M_x$ is the bending moment in the specimen mid-point, $I_{xx}$ is the moment of inertia of the cross-section and $h$ the specimen height.

$$\sigma_a = \frac{M_x}{I_{xx}} \frac{h}{2} \tag{5}$$

*2.4. Micro–CT scan*

Two extra specimens, one for each batch are selected to be scanned and analysed by applying metrological micro-CT techniques [28]. These analyses are conducted before and after the fatigue testing to detect the crack locations and the cracks initiations sites. The specimen loading condition is set to promote the specimen failure at $1 \times 10^6$ cycles.

The authors propose the following notation: the specimen taken from the control batch is indicated as specimen "A", the one from the optimised batch is specimen "B". The specimens were scanned by means of a metrological CT system (Nikon Metrology MCT225), using an optimised single set of scanning parameters, listed in Table 1. The 3D reconstructions are performed using the filtered backprojection algorithm implemented in the software CTPro 3D (Nikon Metrology, UK). The surface determination and the dimensional measurements are conducted using the analysis and visualisation software VGStudio MAX 3.2 (Volume Graphics GmbH, Germany).

## 3. Results and discussion

*3.1. Fatigue behaviour of miniaturised specimens*

The plot in Fig. 5A presents the semi-logarithmic representation of the S-N fatigue curves for four different building orientations. The stress amplitude ($\sigma_a$) was determined by considering the linear section of the gauge length and the nominal cross-sectional area of the strut-junction specimens. The results highlight the impact of the building orientation on the fatigue strength of the strut-junction. The vertically printed specimens (at 90°) showed the lowest fatigue life with $10^7$ cycles and a stress amplitude of 41.2 MPa at the 50 % failure probability. Conversely, as the building orientation decreased, the fatigue life increased, with the highest value of 66.4 MPa reported for the 15° orientation. A summary of these findings can be found in Table 2.

A correlation model, aimed to directly relate the fatigue properties with the strut elevation angle, has been built by a third-grade polynomial fitting of the experimental points (see Table 2). The resulting function is plotted in Fig. 5B and can be utilized to determine the fatigue life of each strut within the lattice structure over a range of 0° to 90°. Due to the three-point-bending loading configuration, the struts in the analysed specimens are subjected to compression-compression (R = 10) or tension–tension (R = 0.1) loading conditions. The stress ratio R = 0.1 is the most critical fati-

**Table 1**
CT scanning parameters adopted in the experimental study.

| Scan parameters | | | | | | |
|---|---|---|---|---|---|---|
| Voltage - kV | Current - μA | Exposure time - s | Frame averaging | Voxel size - μm | Nr. Projections | Cu physical filter - mm |
| 190 | 36 | 2 | 1 | 13 | 3000 | 0.25 |

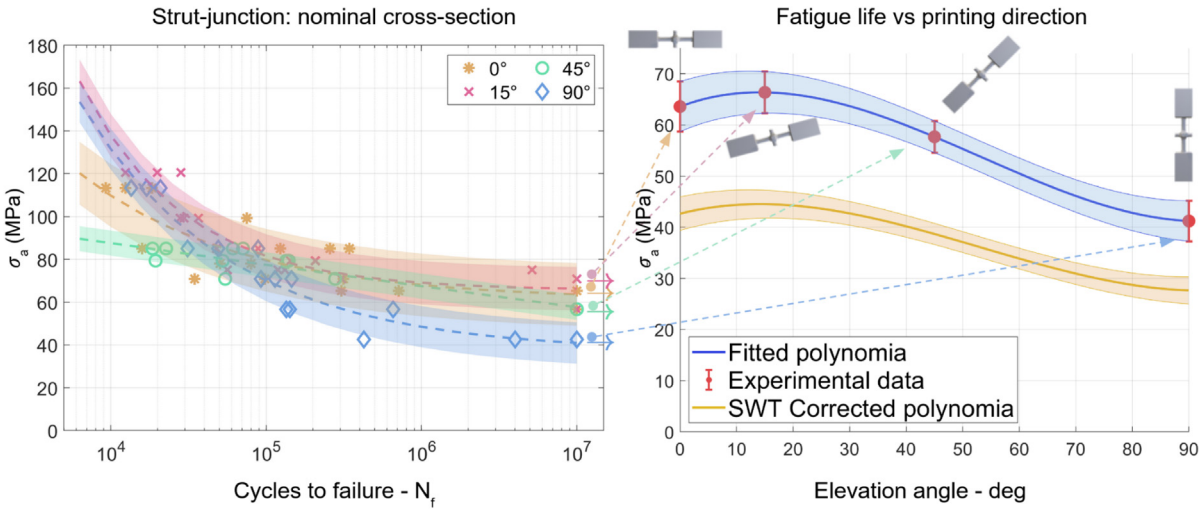


**Fig. 5.** Miniaturised specimens fatigue properties. A: Wöhler curves for miniaturised specimens printed at different elevation angles; B: Experimental fatigue resistance at $N_f = 10^7$ vs printing angle. Experimental data are fitted, and the obtained curve is corrected for the load factor using the SWT coefficient.

**Table 2**
Fitting coefficients for the fatigue curves of miniaturised specimens.

| Elevation angle - deg | C1 | C2 | C3 | $\sigma_a$, 50 % at $10^7$ cycles - MPa | Scatter - MPa |
|---|---|---|---|---|---|
| 0 | 60.94 | 2304.95 | 0.42 | 63.6 | 4.9 |
| 15 | 65.53 | 29575.57 | 0.65 | 66.4 | 4.1 |
| 45 | −688.93 | 818.44 | 0.0057 | 57.7 | 3.1 |
| 90 | 36.83 | 6209.74 | 0.45 | 41.2 | 4.0 |

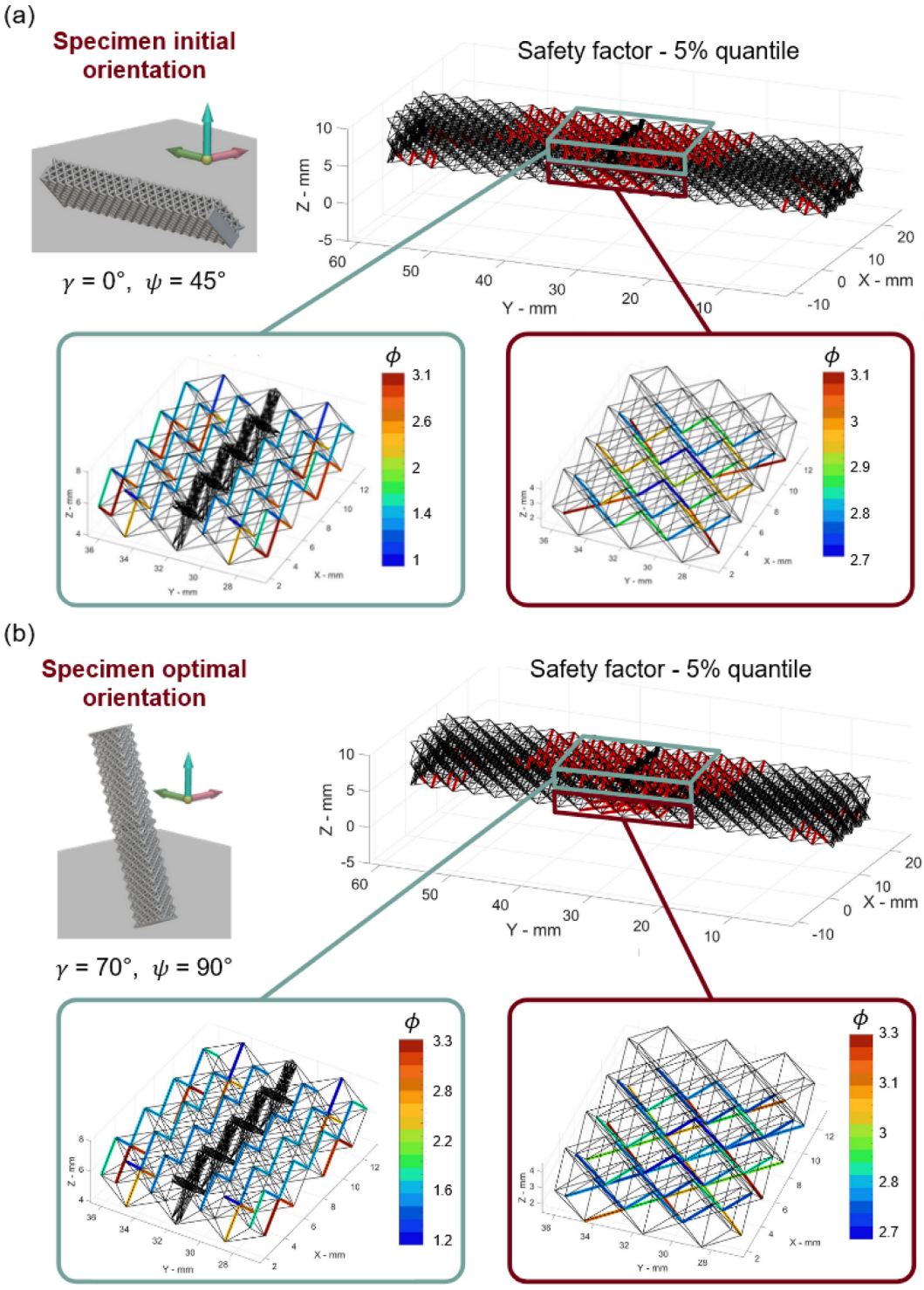


**Fig. 6.** Most critical struts in the three-point-bending specimen are detected using the 5 % quantile for initial (6a) and optimal (6b) configurations. A detailed analysis of the safety factors in the upper and lower regions are presented.

gue regime, due to the crack-opening effect of tensile loads. As a matter of fact, in this regime, a higher predominancy of crack nucleation and propagation from surface defects is generally detected [29]. To match this condition, the curve expressing the fatigue strength for miniaturized specimens at R = −1 is then converted into an equivalent curve expressing the fatigue at R = 0.1. For this purpose, the well-known Smith-Watson-Topper (SWT) approach [30] was adopted since it had been proved to express with a good accuracy the mean stress sensitivity of the fatigue behaviour of L-PBF Ti-6Al-4 V [31]. Specifically, the stress amplitude $\sigma_{a,0.1}$ at R = 0.1 leading to the same number of cycles to failure as $\sigma_{a,-1}$ corresponding to fully-reversed fatigue tests is expressed by:

$$\sigma_{a,0.1} = \sigma_{a,-1}\sqrt{\frac{1-0.1}{2}} \tag{6}$$

The expected dependency of $\sigma_{a,0.1}$ at $1 \times 10^7$ cycles vs. the building angle is shown in Fig. 5B (yellow curve). The 10 %–90 % scatter band is inferred by scaling the standard deviation of the R = −1 curve by the same SWT factor.

### 3.2. Optimization process results

To fully formulate the optimization problem for the case of the three-point bending specimen, a minimum safety factor against fatigue has been set equal to $\phi^* = 1.1$, and the domains of the design variables $\gamma$ and $\psi$, respectively equal to S = [0°;90°] and S' = [0°;90°]. The initial condition for the optimization process is, $\gamma = 0°$ and $\psi = 45°$, based on the printing experience gained by the partner company to reduce the number of printing supports.

The FE simulations in all cases showed that the most critical lattice struts are subjected to tensile loading, making the struts more prone to fatigue failure rather than buckling. Fatigue is a localized and statistical phenomenon, and not only the strut load but also local geometric variations such as manufacturing imperfections play a role in the crack nucleation process. To identify the most likely crack nucleation sites, a set of struts with the lowest fatigue safety factor was selected based on truss-based FE simulations. The 5 % most critical struts were then investigated, as shown in Fig. 6.

The analysis revealed two main potential critical failure areas: an upper and a lower region, represented by the light blue and red boxes in Fig. 6. The FE simulation initially identified a strut located in the upper part of the specimen near the junction with the central reinforcement as the most critical. This strut is oriented at 90° to the job plate, which is the less convenient printing direction as indicated by the function in Fig. 5B.

At the end of the optimization process, the specimen orientation able to maximise the fatigue life is found to be at $\gamma = 70°$ and $\psi = 90°$. This configuration, depicted in Fig. 6, is able to increase the expected fatigue life of the specimen by 60 %. As proposed for the initial configuration, the 5 % quantile was taken into account. The two previously identified regions still contain the most critical struts, so failure is expected to occur in these locations. Upon analysing the specimen printed in the novel configuration, the most critical strut was found to be the same as the one identified in the initial configuration. However, its safety factor against fatigue has increased due to the more favourable printing orientation. The angle of elevation relative to the printing plane for this strut is 20°, close to the maximum resistance identified in the micro-specimen experimental trials as shown in Fig. 5.

In Fig. 7, two curves are displayed. The blue S-N curve represents the control batch, serving as a reference benchmark, and the orange curve represents the optimized batch. The optimized batch demonstrates a higher fatigue life compared to the control batch. In fact, at $10^7$ cycles, a noticeable improvement in fatigue performance, equal to +24 %, is observed in the optimized batch. The main fatigue data are also summarised in Table 3. The reader can directly access the fatigue data of Fig. 7 in the Supplementary materials, Appendix B, Table B1.

Two additional experimental data points are depicted in Fig. 7 with dark red arrows, representing Specimen A and B, which were analysed using micro-CT. The FE estimate of fatigue life is also shown, but these curves do not match the experimental data, which show improved fatigue resistance. Despite this discrepancy, the simulated curves follow the trend of the experimental S-N fatigue curves, and both indicate an improvement in fatigue life for the optimized batch.

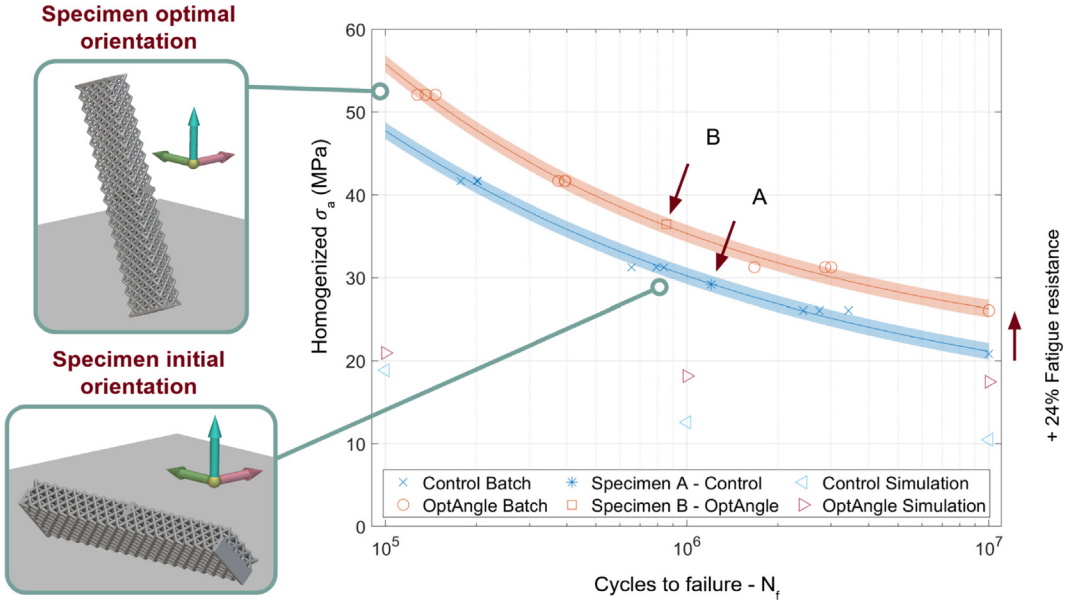


**Fig. 7.** Wöhler curves for three-point-bending specimens, where $\sigma_a$ represent the homogenised maximum bending stress amplitude as computed in Equation (5). Experimental data are followed by the expected ones computed using FE simulations. The dark red arrows mark the specimens A and B analysed with the micro-CT technology.

**Table 3**
Fitting coefficients for the three-point-bending fatigue tests.

| Elevation angle - deg | C1 | C2 | C3 | $\sigma_{a,50\%}$ at $10^7$ cycles - MPa | Scatter - MPa |
|---|---|---|---|---|---|
| Control | 0.0552 | 4.7308 | 0.2869 | 21.2 | 1.0 |
| Optimised | 0.0918 | 10.5217 | 0.3552 | 26.3 | 1.0 |

While a precise fatigue life estimation is challenging to achieve with a simplified model, the improvement in performance of the optimized batch is a noteworthy result that demonstrates the efficacy of the optimization method. However, the outcome is not consistent with expectations, suggesting that an important factor may be missing in the fatigue life assessment. To further understand the mismatch, micro-CT scans of the specimens are being considered.

### 3.3. Micro-CT characterization

The micro-CT 3D reconstructions are analysed to assess the true geometry of the specimens and identify the failure locations. Both specimens A and B undergo visual inspection and a detailed metrological analysis of specific points of interest. The micro-CT reconstructions are compared with the nominal geometry used in the printing process, and both specimens show a significant difference between the actual and intended geometry. The struts exhibit manufacturing-induced defects such as partially melted powder, surface irregularities, and internal porosity, affecting their geometry. Some struts also have structural deviations in the form of waviness, as illustrated in Fig. 8A.

Two volumes, each containing an Octet Truss cell, are selected from the specimens to examine the most critical struts as identified in the analysis of the 5 % quantile in Fig. 6. The first volume is located in the upper region, while the second is in the lower region, as depicted in Fig. 8A. The lattice geometry in the selected volumes is analysed in depth to investigate crack position and nucleation causes, access internal porosity, and compute struts cross-sectional areas. The cross-sectional areas are determined by fitting a cylinder to the surface of each reconstructed strut using Gaussian fitting. The cylinder fit is also used to determine the strut elevation angle relative to the printing plane. The measurement results are presented in the Supplementary materials, Appendix B, Table B2.

The struts' cross-section can be divided into different batches based on the elevation angle relative to the printing plane, as shown in Fig. 9. Specimens A and B have different batches of cross-sectional areas, reflecting their different orientation relative

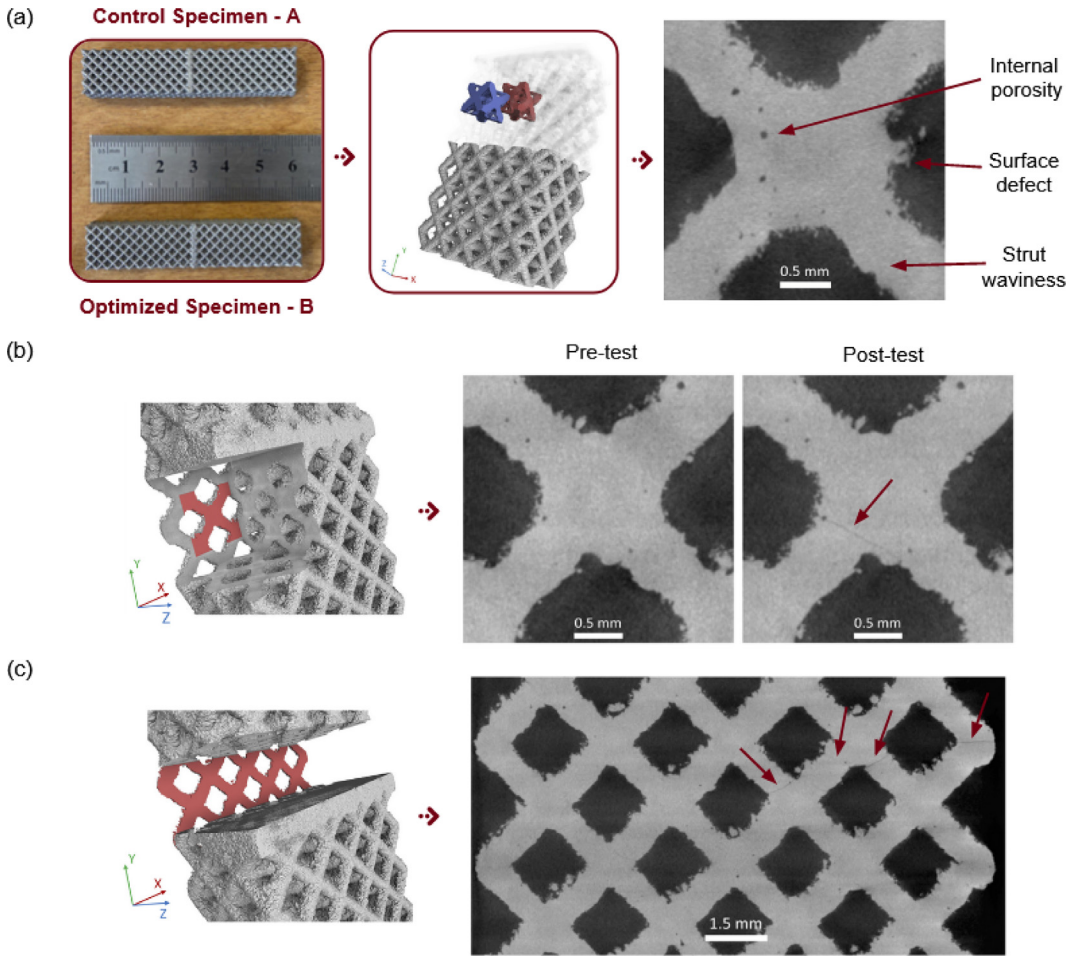


**Fig. 8.** Micro-CT analysis of the three-point-bending specimens. A: Specimens A and B underwent the micro-CT analysis. A 3D reconstruction of a specimen and in blue and red the OT cells selected for in depth analysis. A detail of a lattice struts shows the manufacturing induced defects; B: Pre- and post-test comparison of a critical strut in the lower region of the specimen. A crack nucleated near the node junction clearly originating from a surface defect and crossing an internal porosity. C: Crack distribution in the lower region of the specimens.

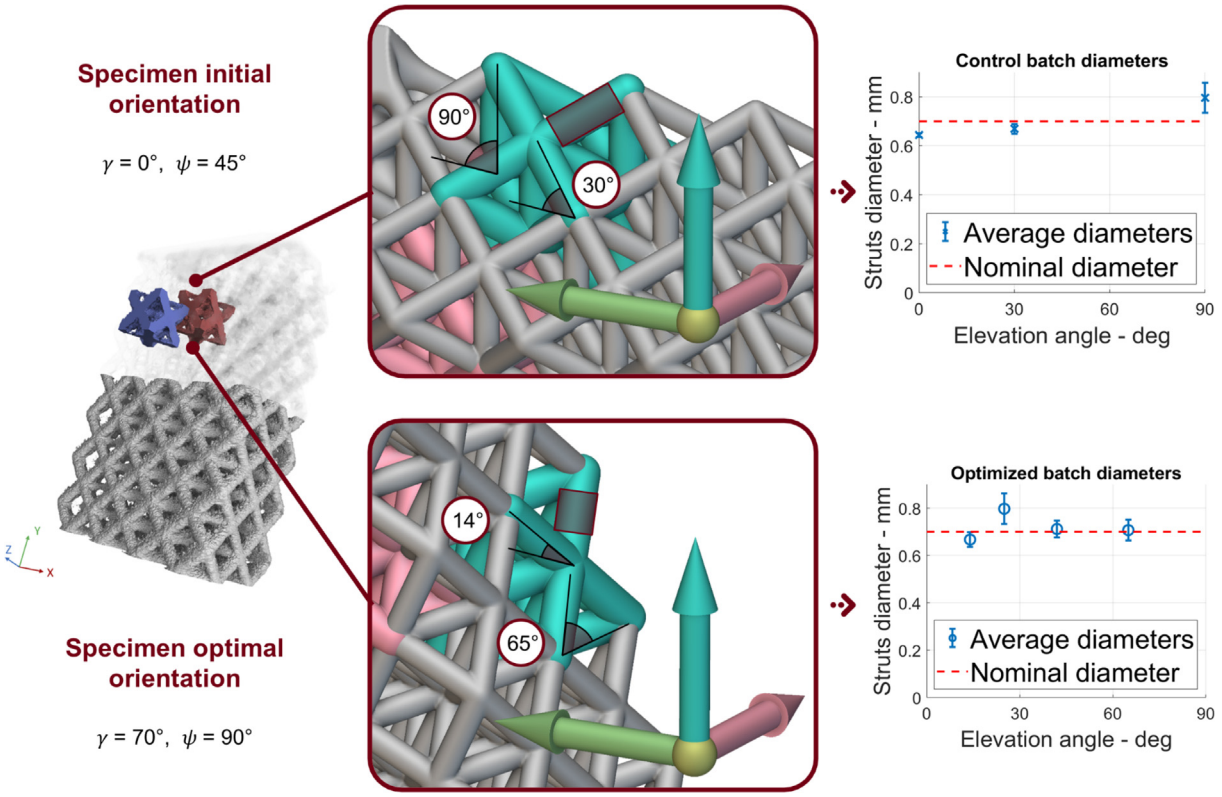


**Fig. 9.** Metrological analysis of the lattice struts in the highlighted volumes. Cross-sectional areas are divided into different batches based on the elevation angle with respect to the printing plane.

to the printing plane. The measurements clearly show that the cross-sectional area deviates from the intended design, and the deviation depends on the elevation angle relative to the printing plane. This factor influences the specimen's fatigue resistance and should be considered in the fatigue life estimation.

The geometry of the specimens remained unchanged after the fatigue tests except for the presence of fatigue-induced cracks on various struts in both specimens A and B, as illustrated in Fig. 8B.

For both specimens, multiple failed struts are found in the lower region of the specimen; the cracks always nucleate from a clearly visible surface defect and most of the time propagate through at least one internal pore, as visible in the example in Fig. 8B. The similarities between the two specimens also include the crack positions. As shown in Fig. 8C, several cracks pass through the entire specimen from left to right, for both specimens A and B, engaging different strut layers. These cracks are most of the time localised near the nodes or cross the struts in the node proximity. The failed struts undergo tensile loads promoting a fatigue failure driven by the surface irregularities and the internal porosity effect.

The upper region of the specimens was also analysed, and it was found that the presence of manufacturing-induced defects was consistent with that in the lower region, demonstrating a consistency in the manufacturing quality. Based on the finite element analysis, the most critical strut in the structure was located in this region, but no cracks were found in either of the specimens.

### 3.4. Verification analysis

The distribution of a strut's cross-section depends on its elevation angle, as shown in Fig. 9. To accurately estimate its fatigue life, a verification finite element (FE) analysis is performed. The FE model, based on truss elements, is updated by calculating the elevation angle of each element in the lattice relative to the printing plane. The cross-sectional area of each element is then assigned using the average cross-section found in Fig. 9, corresponding to the computed elevation angle. The results of this analysis are shown in Fig. 10, demonstrating that using the measured average cross-section improves the simulated fatigue resistance. In particular, the estimation at $N_f = 1 \times 10^7$ cycles shows a fatigue resistance double with respect to the experimental results. This phenomenon leads to the important consideration that the real cross-sectional area of struts is crucial for accurate fatigue life prediction in lattice structures. It is recommended to conduct a post-analysis based on the actual strut geometry to access these values. The verification truss model shows improved fatigue resistance compared to the experimental results, but this is understandable as this model does not account for the manufacturing imperfections that negatively impact the real specimen's fatigue performance.

Comparing the experimental results and the simulations computed with the average cross-sectional areas, a fatigue stress concentration factor $K_t = 2$ is computed with the following formula:

$$K_t = \frac{\sigma_{Simulated}}{\sigma_{Experimental}} \tag{7}$$

This coefficient links the simulated axial load and the allowable load in the struts. This value is computed a posteriori and considers the detrimental effect of the manufacturing induced defects on the lattice fatigue life estimation. Lastly, a novel evaluation of the improvement given by the optimised batch is computed. The optimised set is estimated to have a +15 % improvement in the fatigue life with respect to the simulated control batch. This new value is coherent with the experimental results.

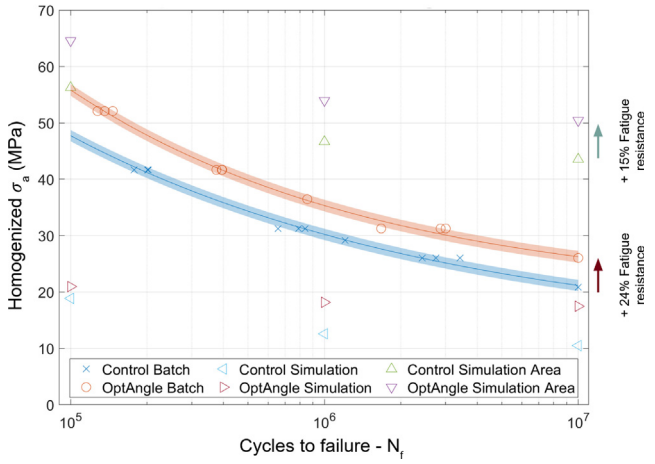


**Fig. 10.** Wöhler curves of the three-point-bending specimens with the a-posteriori fatigue life estimations based on the micro-CT metrological analysis.

## 4. Conclusions

The proposed optimization process is designed to enhance the fatigue life of lattice structures by utilizing a truss model that is computationally efficient and has industrial relevance. In order to verify the efficacy of this process, a series of experiments, micro-CT scans, and FE analyses were conducted. The results of these studies showed that the optimization framework was able to significantly increase the fatigue life of the specimens, both in simulated and experimental conditions. The simulations indicated an improvement of 60 %, while the real specimens showed an improvement of 24 %. This difference can be attributed to the assumptions made during the modelling process.

The micro-CT scans were used to examine the deviations between the ideal and real geometries of the specimens. Additionally, an a posteriori FE analysis was performed to consider the effective strut cross-sections, which improved the estimation of the fatigue life. Although this work does not provide a formal prediction of the fatigue life of lattice structures based on miniaturized specimens, an approximate result was obtained using the computationally efficient FE truss model.

The results of the experiments showed that the fatigue estimation based on the computation of axial stress within the struts was able to distinguish the potential failure mechanisms. The experiments showed that the specimens failed due to fatigue loading and no buckling phenomena were observed. The micro-CT analysis revealed that the locations of crack nucleation were primarily near the nodes and were associated with surface defects and internal porosity. The failed struts were found to be located in the lower region of the specimens due to the high concentration of critical struts in this area.

The statistical analysis, which was based on the detection of the quantile containing the 5 % most critical struts, was able to identify the probable failure locations in the specimens. The micro-CT analysis revealed that manufacturing-induced defects have a significant impact on the geometry of the specimens, including surface irregularities, internal porosity, and waviness in the struts. Additionally, the manufacturing process also influences the definition of the strut cross-sectional areas.

The proposed optimization algorithm is general in purpose, nevertheless, the reader should be aware of the work limitations. Fatigue life properties can be influenced by lattice topology or its geometrical dimensions. Factors such as strut diameter, the presence of fillet radii or variation in porosity can change the relationship between fatigue life and printing direction. Moreover, also the influence of post-processing steps such as, heat or surface treatments should be considered with care. Cost effective experimental campaign on miniaturized specimens should be therefore performed to retrieve the novel relation.

In the future, the authors plan to further develop a complete fatigue life estimation based on the data from miniaturized specimens. This will be accomplished by taking into account the statistical nature of the fatigue phenomenon, which will lead to a statistical optimization framework. The authors also plan to use micro-specimen metrological assessments to transfer information about defect characteristics and effective cross-sectional areas to the lattice struts.

## Data availability

Data will be made available on request.

## Declaration of Competing Interest

The authors declare the following financial interests/personal relationships which may be considered as potential competing interests: [Raffaele De Biasi reports equipment, drugs, or supplies was provided by Lincotek Additive (Pergine Valsugana, Italy). Simone Murchio reports equipment, drugs, or supplies was provided by Lincotek Additive (Pergine Valsugana, Italy). This project was supported by the Italian Ministry of Education, University, and Research (MIUR) within the program "Departments of Excellence" 2018–2022 (DII-UNITN).].

## Acknowledgements

The authors want to thank Gianluca Zappini form Lincotek Additive (Pergine Valsugana, Italy) for his contribution in the proof reading of the manuscript.

## Appendix A. Supplementary material

Supplementary data to this article can be found online at https://doi.org/10.1016/j.matdes.2023.111975.

## References

[1] L. Riva, P.S. Ginestra, E. Ceretti, Mechanical characterization and properties of laser-based powder bed-fused lattice structures: a review, Int. J. Adv. Manuf. Technol. 113 (2021) 649–671, https://doi.org/10.1007/s00170-021-06631-4.
[2] A. Vigliotti, D. Pasini, Stiffness and strength of tridimensional periodic lattices, Comput. Methods Appl. Mech. Eng. 229–232 (2012) 27–43, https://doi.org/10.1016/j.cma.2012.03.018.
[3] P. Köhnen, C. Haase, J. Bültmann, S. Ziegler, J.H. Schleifenbaum, W. Bleck, Mechanical properties and deformation behavior of additively manufactured lattice structures of stainless steel, Mater. Des. 145 (2018) 205–217, https://doi.org/10.1016/j.matdes.2018.02.062.
[4] A. Mirabolghasemi, A.H. Akbarzadeh, D. Rodrigue, D. Therriault, Thermal conductivity of architected cellular metamaterials, Acta Mater. 174 (2019) 61–80, https://doi.org/10.1016/j.actamat.2019.04.061.
[5] A. du Plessis, I. Yadroitsava, I. Yadroitsev, S.G. le Roux, D.C. Blaine, Numerical comparison of lattice unit cell designs for medical implants by additive manufacturing, Virtual Phys. Prototyp. 13 (2018) 266–281, https://doi.org/10.1080/17452759.2018.1491713.
[6] V.S. Deshpande, M.F. Ashby, N.A. Fleck, Foam topology: bending versus stretching dominated architectures, Acta Mater. 49 (6) (2001) 1035–1040.
[7] Y.J. Liu, D.C. Ren, S.J. Li, H. Wang, L.C. Zhang, T.B. Sercombe, Enhanced fatigue characteristics of a topology-optimized porous titanium structure produced by selective laser melting, Addit. Manuf. (2020) 32, https://doi.org/10.1016/j.addma.2020.101060.
[8] D. Mahmoud, M.A. Elbestawi, Lattice structures and functionally graded materials applications in additive manufacturing of orthopedic implants: A review, J. Manuf. Mater. Process. (2017) 1, https://doi.org/10.3390/jmmp1020013.
[9] B. Blakey-Milner, P. Gradl, G. Snedden, M. Brooks, J. Pitot, E. Lopez, M. Leary, F. Berto, A. du Plessis, Metal additive manufacturing in aerospace: A review, Mater Des 209 (2021) 110008, https://doi.org/10.1016/j.matdes.2021.110008.

[10] M. Benedetti, A. du Plessis, R.O. Ritchie, M. Dallago, S.M.J. Razavi, F. Berto, Architected cellular materials: A review on their mechanical properties towards fatigue-tolerant design and fabrication, Mater. Sci. Eng. R. Rep. (2021) 144, https://doi.org/10.1016/j.mser.2021.100606.
[11] R.M. Latture, R.X. Rodriguez, L.R. Holmes, F.W. Zok, Effects of nodal fillets and external boundaries on compressive response of an octet truss, Acta Mater. 149 (2018) 78–87, https://doi.org/10.1016/j.actamat.2017.12.060.
[12] I. Echeta, X. Feng, B. Dutton, R. Leach, S. Piano, Review of defects in lattice structures manufactured by powder bed fusion, Int. J. Adv. Manuf. Technol. 106 (2020) 2649–2668, https://doi.org/10.1007/s00170-019-04753-4.
[13] N. Sanaei, A. Fatemi, Defects in additive manufactured metals and their effect on fatigue performance: A state-of-the-art review, Prog. Mater. Sci. (2021) 117, https://doi.org/10.1016/j.pmatsci.2020.100724.
[14] J. Pegues, M. Roach, R. Scott Williamson, N. Shamsaei, Surface roughness effects on the fatigue strength of additively manufactured Ti-6Al-4V, Int. J. Fatigue 116 (2018) 543–552, https://doi.org/10.1016/j.ijfatigue.2018.07.013.
[15] U. Zerbst, M. Madia, C. Klinger, D. Bettge, Y. Murakami, Defects as a root cause of fatigue failure of metallic components. III: Cavities, dents, corrosion pits, scratches, Eng. Fail Anal. 97 (2019) 759–776, https://doi.org/10.1016/j.engfailanal.2019.01.034.
[16] T. Persenot, A. Burr, G. Martin, J.Y. Buffiere, R. Dendievel, E. Maire, Effect of build orientation on the fatigue properties of as-built Electron Beam Melted Ti-6Al-4V alloy, Int. J. Fatigue 118 (2019) 65–76, https://doi.org/10.1016/j.ijfatigue.2018.08.006.
[17] T. Maconachie, M. Leary, B. Lozanovski, X. Zhang, M.a. Qian, O. Faruque, M. Brandt, SLM lattice structures: Properties, performance, applications and challenges, Mater. Des. 183 (2019) 108137, https://doi.org/10.1016/j.matdes.2019.108137.
[18] G. Strano, L. Hao, R.M. Everson, K.E. Evans, Surface roughness analysis, modelling and prediction in selective laser melting, J. Mater. Process Technol. 213 (2013) 589–597, https://doi.org/10.1016/j.jmatprotec.2012.11.011.
[19] G. Savio, R. Meneghello, G. Concheri, Optimization of lattice structures for additive manufacturing technologies, Lecture Notes Mech. Eng. (2017) 213–222, https://doi.org/10.1007/978-3-319-45781-9_22.
[20] L. Cheng, P. Zhang, E. Biyikli, J. Bai, J. Robbins, A. To, Efficient design optimization of variable-density cellular structures for additive manufacturing: Theory and experimental validation, Rapid Prototyp. J. 23 (2017) 660–677, https://doi.org/10.1108/RPJ-04-2016-0069.
[21] S. Arabnejad Khanoki, D. Pasini, Multiscale design and multiobjective optimization of orthopedic hip implants with functionally graded cellular material, J. Biomech. Eng. (2012) 134, https://doi.org/10.1115/1.4006115.
[22] R.R. Fernandes, A.Y. Tamijani, Design optimization of lattice structures with stress constraints, Mater. Des. (2021) 210, https://doi.org/10.1016/j.matdes.2021.110026.
[23] R.M. Gorguluarslan, U.N. Gandhi, Y. Song, S.K. Choi, An improved lattice structure design optimization framework considering additive manufacturing constraints, Rapid Prototyp. J. 23 (2017) 305–319, https://doi.org/10.1108/RPJ-10-2015-0139.
[24] S. Murchio, M. Dallago, A. Rigatti, V. Luchin, F. Berto, D. Maniglio, M. Benedetti, On the effect of the node and building orientation on the fatigue behavior of L-PBF Ti6Al4V lattice structure sub-unital elements, Mater. Design Process. Commun. 3 (6) (2021), https://doi.org/10.1002/mdp2.258.
[25] S. Murchio, M. Dallago, F. Zanini, S. Carmignato, G. Zappini, F. Berto, D. Maniglio, M. Benedetti, Additively manufactured Ti–6Al–4V thin struts via laser powder bed fusion: Effect of building orientation on geometrical accuracy and mechanical properties, J. Mech. Behav. Biomed. Mater. 119 (2021) 104495, https://doi.org/10.1016/j.jmbbm.2021.104495.
[26] V.S. Deshpande, N.A. Fleck, M.F. Ashby, Effective properties of the octet-truss lattice material, Effect. Prop. Octet-truss Lattice Mater. 49 (8) (2001) 1747–1769.
[27] L. Emanuelli, A. Molinari, L. Facchini, E. Sbettega, S. Carmignato, M. Bandini, M. Benedetti, Effect of heat treatment temperature and turning residual stresses on the plain and notch fatigue strength of Ti-6Al-4V additively manufactured via laser powder bed fusion, Int. J. Fatigue 162 (2022) 107009, https://doi.org/10.1016/j.ijfatigue.2022.107009.
[28] S. Carmignato, W. Dewulf, R. Leach, Industrial X-ray computed tomography, Springer International Publishing, 2017, https://doi.org/10.1007/978-3-319-59573-3.
[29] C.N. Kelly, C. Kahra, H.J. Maier, K. Gall, Processing, structure, and properties of additively manufactured titanium scaffolds with gyroid-sheet architecture, Addit. Manuf. (2021) 41, https://doi.org/10.1016/j.addma.2021.101916.
[30] K. Smith, P. Watson, T. Topper, A stress–strain parameter for the fatigue of metals, J. Mater. 5 (1970) 767–778.
[31] M. Benedetti, V. Fontanari, M. Bandini, F. Zanini, S. Carmignato, Low- and high-cycle fatigue resistance of Ti-6Al-4V ELI additively manufactured via selective laser melting: Mean stress and defect sensitivity, Int. J. Fatigue 107 (2018) 96–109, https://doi.org/10.1016/j.ijfatigue.2017.10.021.